Journal of Applied Polymer Science

Hybrid Polyaniline–TiO_2 Nanocomposite Langmuir–Blodgett Thin Films: Self-Assembly and Their Characterization

Gurpreet Kaur Bhullar, Ramneek Kaur, K. K. Raina
Materials Research Laboratory, School of Physics and Materials Science, Thapar University, Patiala 147004, Punjab, India
Correspondence to: K. K. Raina (E-mail: kkraina@gmail.com)

ABSTRACT: Polyaniline (PANi)–titanium dioxide (TiO_2) nanocomposite materials were prepared by chemical polymerization of aniline doped with TiO_2 nanoparticles. Surface pressure–area (π-A) isotherms of these nanocomposites show phase transformations in the monolayer during compression process. Multiple isotherms indicate that the monolayer of the nanocomposite material can retain its configuration during compression-expansion cycles. Langmuir–Blodgett thin films of PANi–TiO_2 nanocomposite were deposited on the quartz and indium tin oxide coated conducting glass substrates. Fourier transfer infrared spectroscopy and UV–visible spectroscopy study indicates the presence of TiO_2 in PANi, whereas X-ray Diffraction study confirmed the anatase phase of TiO_2 and particle size (∼nm) of PANi–TiO_2. The morphology of Langmuir–Blodgett films of these nanocomposites was also characterized by atomic force microscopy. © 2014 Wiley Periodicals, Inc. J. Appl. Polym. Sci. **2015**, *132*, 41386.

KEYWORDS: composites; conducting polymers; microscopy; self-assembly; surfaces and interfaces

Received 13 December 2013; accepted 9 August 2014
DOI: 10.1002/app.41386

INTRODUCTION

Conducting polymers have emerged as novel electronic materials considering their use in molecular electronic devices. These materials possess the electronic properties of semiconductors as well as the flexible behavior of polymers.[1–6] Amongst the family of conducting polymers, polyaniline (PANi) has special characteristic due to the presence of reactive —NH— groups in a polymer chain, which imparts hydrophilic character to the system, relatively high conductivity, and good chemical stability.[7,8]

The electronic properties of the conducting polymers can further be enhanced by tailoring them with metal oxides. Titanium dioxide (TiO_2) being nontoxic, insoluble, inexpensive, and chemically stable, emerged as one of the most suitable doping agents in PANi. The preparation of PANi–TiO_2 nanocomposites is standardized because of their well-matched band gap for the charge transfer. TiO_2 anatase is a typical n-type wide gap semiconductor (∼3.2 eV), whereas PANi is considered to be a p-type material having a wide band gap (∼3.6 eV). It has been observed that the n-p contacts between TiO_2 and PANi matrix gives rise to variety of shallow donors and acceptor levels increasing the physical adsorption sites for gas molecules thus enhancing the gas sensing features of PANi–TiO_2 nanocomposites.[9–11] Some recent reports show that these materials have also been applied in newer applications like electrically conductive textiles, gas sensor, and photosensing applications with their reasonable photocatalytic and enhanced optical activity etc.[12–17]

The metal/organic semiconductor materials are expected to be substitutes of the metal/inorganic semiconductor junctions in order to provide low-cost flexible electronic devices.[18–20]

Langmuir–Blodgett (LB) method offers a novel and relatively simple method of producing ultra-thin films, with fine control over film thickness. Density, film thickness, and homogeneity are preserved in the LB films, giving the possibility to make self-assembled multilayer structures with varying layer compositions. It also facilitates to prepare single molecule thin electronic device from nano- or micro-sized metal particles or rods using this technique. Spin casting is also a good deposition technique for organic molecules but film thickness is relatively high as compared with LB films. This technique is usually used for bottom up assembly in nanotechnology and functional materials applications at room temperature. In Langmuir films, the interactions between hydrophobic and hydrophilic moieties determine the molecular orientation. The required amphiphilicity of PANi is provided by the presence of —NH— groups, benzoid and quinoid rings in a polymer chain. Thus, several research groups made attempts to investigate thin films behavior of conducting polymers using LB technique with PANi getting special attention,[21–24] but the behavior of Langmuir monolayer and LB films of PANi–TiO_2 nanocomposite systems is still infancy.

In this article, we report on the preparation of hybrid PANi–TiO_2 nanocomposite materials by chemical route and depositing their thin films by LB method. We made an attempt to understand

© 2014 Wiley Periodicals, Inc.

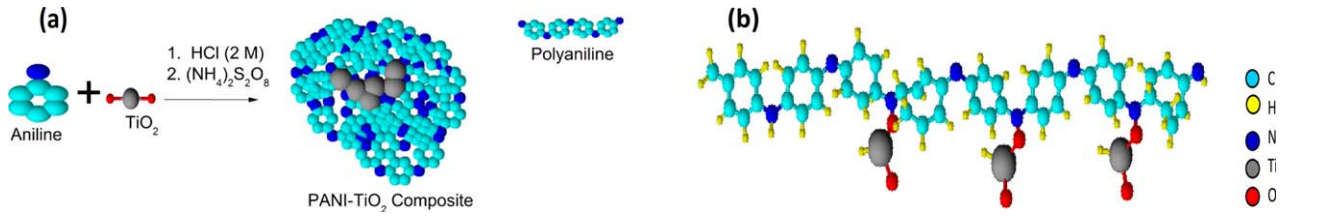

Figure 1. (a) Schematic of the reaction mechanism for PANi–TiO_2 nanocomposite showing polymerization occur over the surface of TiO_2 nanoparticles, and (b) molecular model representing the position of TiO_2 in the PANi chain molecules as sketched using ACD Chem software. [Color figure can be viewed in the online issue, which is available at wileyonlinelibrary.com.]

their properties at air–water and air–solid interfaces and study their morphology.

EXPERIMENTAL

Materials

Aniline (LR for synthesis, purity 99%) and acetone (Guaranteed grade, purity 99.5%) were purchased from M/S Loba chemie, ammonium persulfate (APS) $(NH_4)_2S_2O_8$ (AR, purity 98.5%), *N*-methylpyrrolidone (NMP) (LR, purity 99.5%), TiO_2 (25 nm) from Degussa P-25, hydrochloric acid, and sodium hydroxide (AR) were purchased from M/S S. D. fine-chemicals, and Ethanol (AR, purity 99.9%) from Merck were used without further purification. Milli-Q filtered (Direct Q_3) deionized and ultrapure water (Resistivity = 18.2 MΩ cm) was used for synthesis of nanocomposites and for preparing subphase.

Preparation of PANi–TiO_2 Hybrid Nanocomposites

PANi–TiO_2 nanocomposite systems were prepared by chemical route. Aniline (1.6 mL) was injected for the dispersion of 50 mL of 2*M* HCl containing TiO_2 powder under ultrasonic action to avoid the agglomeration of TiO_2 nanoparticles. After 30 min, APS was mixed into this dispersion system with constant stirring and keeping the temperature of the reaction system between 0 and 5°C. The resulting mixture was allowed to react for 10 h at room temperature. The precipitated powder was filtered by using Millipore vacuum filter (pore size ~0.22 μm) and washed with deionized water to remove the unreacted aniline monomer. These nanocomposites with different concentration of TiO_2 were doped by treating with 1 L of 1*M* HCl solution. PANi was prepared by similar procedure in the absence of TiO_2. The final compound was dried in vacuum at 40°C for 24 h. The molar ratios of aniline to HCl and to APS for either PANi or PANi–TiO_2 nanocomposites were retained at 1 : 0.5 and 1 : 1, respectively.[11]

The reaction mechanism for PANi–TiO_2 nanocomposite showing polymerization of aniline on the surface of TiO_2 nanoparticles is shown in Figure 1(a). The average molecular length of monomer was ~5 Å (as determined from its molecular structure). Figure 1(b) shows the molecular model representing the position of TiO_2 in the PANi chain molecules as sketched using ACD Chem software.

Langmuir–Blodgett Films of PANi and PANi–TiO_2 Composite

The experimental set up for LB film deposition essentially consists of a mini-trough (KSV-NIMA, Finland). The trough was thoroughly cleaned with ethanol followed by deionized water to ensure impurity free subphase for monolayer. The spreading solution of PANi and PANi–TiO_2 (20 wt %) was prepared in NMP and particle concentration is 0.2 mg/mL. A total of 200 μL of the solution was spread on the ultrapure Milli-Q_3 (pH = 6.00) water subphase contained in trough by using Hamilton micro syringe. The density of NMP was higher than that of water, so it got settled down at the bottom of subphase leaving behind the composite material to be deposited, on water surface.[25,26] The solvent settled down in about 30 min before the area enclosed by the barriers (derlin) was reduced at 10 mm min^{-1} to compress the molecules on the water surface.

Indium tin oxide (ITO) coated conducting glass and quartz substrates were used for thin film deposition. ITO-coated glass was cleaned with acetone, ultrasonicated for about half an hour in 10% aqueous solution of sodium hydroxide, and rinsed in deionized water for about 10 min. The substrate was dried and then clamped to the dipper. LB films were deposited on substrates using the vertical dipping method at 0.5 mm min^{-1} downstroke and 2.0 mm min^{-1} upstroke, respectively. The depositions were made at a constant pressure of 10 mN m^{-1}, and started from above the surface after 10 min of stabilization. The deposited film was dried for about 5 min and then placed in vacuum desiccator to ensure moisture free environment. Quartz substrate was cleaned by washing with acetone followed by deionized water and process repeated to deposit thin films.

RESULTS AND DISCUSSION

Fourier Transfer Infrared Spectroscopy

Fourier transfer infrared (FTIR) spectroscopy profile of PANi, TiO_2, and PANi–TiO_2 nanocomposites (5, 10, 15, 20 wt %) is shown in Figure 2. The measurements were carried out by FTIR spectroscope (BX-II, Perkin Elmer), resolution 4 cm^{-1}, and no. of scans 16; scan range 400 to 4000 cm^{-1} at room temperature. The main characteristic bands of PANi shown in Figure 2(a) were assigned as follows: the peak at 3456.12 cm^{-1} is attributed to N—H stretching mode, the peaks at 1565 cm^{-1} and 1487 cm^{-1} are associated with C=N and C=C stretching mode for the quinonoid and benzenoid rings, the peaks at about 1299 cm^{-1} is attributed to C—N stretching mode for benzenoid ring, whereas the peak at 1145 cm^{-1} is due to quinonoid unit of doped PANi and the peak at 876 cm^{-1} was assigned to an out-of-plane bending vibration of C—H of 1,4 substituted benzenoid rings, which confirmed the formation of PANi.[27,28] The results show that obtained PANi contain 1,4-para-disubstituted linear chains. Figure 2(b) shows a broad peak between 800 and 465 cm^{-1} assigned to the Ti—O—Ti stretching vibrations with a valley centered at 503 cm^{-1}. The band Ti—OH observed below

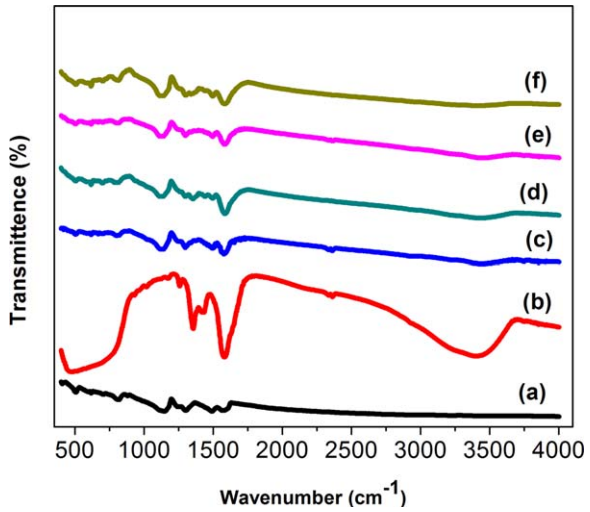

Figure 2. FTIR profile of the (a) PANi, (b) 5, (c) 10, (d) 15, (e) 20 wt % TiO_2 in PANi–TiO_2 nanocomposite, respectively, and (f) Pure TiO_2. [Color figure can be viewed in the online issue, which is available at wileyonlinelibrary.com.]

3500 cm^{-1} indicates the existence of hydrogen bonding.[29] For the PANi–TiO_2 nanocomposites (20 wt %), the characteristic peaks of PANi around 1299 cm^{-1}, 1495 cm^{-1}, and 1581 cm^{-1} shifted to higher wavenumbers of 1301, 1492, and 1575 cm^{-1} after TiO_2 was introduced indicating a slight effect of TiO_2 on the bonds involved in these bands Figure 2(f). The characteristic peak of the N—H stretching mode at 3456 cm^{-1} of PANi shifted to a lower wavenumber (3417 cm^{-1}) in the PANi–TiO_2 nanocomposite, and the hydrogen bond absorption at 3210 cm^{-1} was strengthened after TiO_2 was introduced. Titanium is a transition metal element, so TiO_2 has a strong tendency to form coordinate bond with the nitrogen atoms in PANi.[30] From the spectrum of PANi–TiO_2 nanocomposite, it was realized that a strong interaction exists between PANi and TiO_2 particles, and the polymerization of aniline occurs on the surface of TiO_2 nanoparticles. Similar shifts of peak positions in PANi–TiO_2 (10, 15, 20 wt %) nanocomposites have been observed as shown in Figure 2(c–e).

Monolayer at Air–Water Interface

π-A Isotherms. Figure 3 shows surface pressure–mean molecular area (π-A) isotherm behavior of PANi–TiO_2 (20 wt %) at the air–water interface with constant compression speed at 10 mm min^{-1}. It can be seen clearly that the isotherm has the typical features of LB pressure isotherms. A_i represents lift off area; at this point, compression of monolayer just starts and, with constant compression by using barriers, we reached at condensed phase (A_0).

In region (I), we see minimum change in the surface pressure; monolayer is in the gaseous state starting from lift off area (A_i) ~70.09 $Å^2$/molecule. Surface pressure varies from 0.06 to 0.80 mN m^{-1}. On further compression, monolayer attained expanded liquid phase from gaseous phase as indicated by region (II). A gradual increase in surface pressure up to 10 mN m^{-1} is observed indicating condensed phase of monolayer. Figure 3 (Inset) shows isotherm of PANi taken at constant compression rate 10 mm min^{-1}. The molecules were initially in the gaseous phase (a to b) from lift off area (A_i) ~15.74 $Å^2$/molecule to 13.75 $Å^2$/molecule, surface pressure varied from 0.02 to 0.70 mN m^{-1}. With further compression of barriers, gradual rise was observed in the surface pressure up to 9.6 mN m^{-1}. Thus, molecules had reached to a condensed phase (b to c) due to their molecular arrangement and ordering at air–water interface with compression of barriers. At this stage, the monolayer was compressed to limiting area, A_0 ~ 13.49 $Å^2$.

Doping of 20 wt % TiO_2 in PANi increases both lifting area (A_i) and condensed area (A_0) as seen in Figure 3. It indicates that TiO_2 nanoparticles are influencing the orientation of monolayer of polymer matrix.

The stability of the films over water surface for PANi–TiO_2 (20 wt %) was studied by running three complete cycles in range of (0–10) mN m^{-1} as shown in Figure 4. We found that continuous compression–expansion cycles have negligible hysteresis with almost zero shifting in each cycle. It establishes the stability of the monolayer at water surface, which clearly proved that during compressing of barriers none of the molecule had squeezed out from the water surface. These stable films were easily transferred to substrates by using Y-type deposition method.[31,32]

Monolayer at Air–Solid Interface

Electron Absorption Spectroscopy. Figure 5(i) shows spectra of pure PANi, PANi–TiO_2 (5, 10, 15, 20 wt %) nanocomposites, and TiO_2 nanoparticles in NMP between 300 nm and 1000 nm recorded by using UV–visible spectrophotometer (Analytic Jena, SPECTROD 205). PANi as well as PANi–TiO_2 nanocomposites are soluble properly in NMP. Figure 5(i) indicates that pure TiO_2 absorbs light of wavelengths below 400 nm (UV region) only, whereas PANi and PANi–TiO_2 nanocomposites have broad absorbance in the UV and visible regions. The spectra of PANi show two characteristic bands at 320 nm and 630 nm,

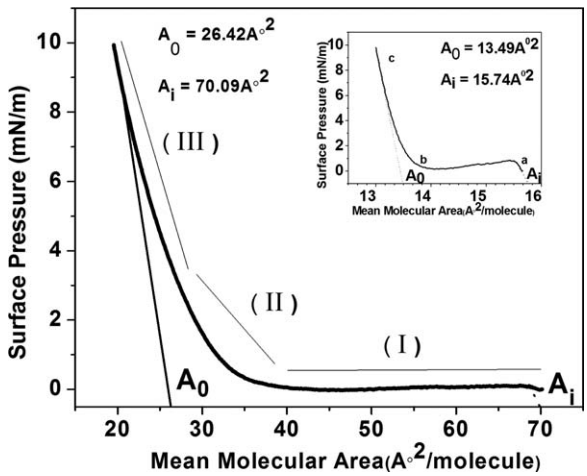

Figure 3. Surface pressure–area isotherm profile of PANi–TiO_2 (20 wt %) nanocomposite monolayer, particle concentration 0.2 mg/mL in NMP solution, spreading amount 200 μL and compressed to target pressure 10 mN/m at 10 mm/min. Inset is the π-A isotherm profile of PANi monolayer, particle concentration 0.2 mg/mL in NMP solution, spreading amount 200 μL, and compressed to target pressure 10 mN/m at 10 mm/min.

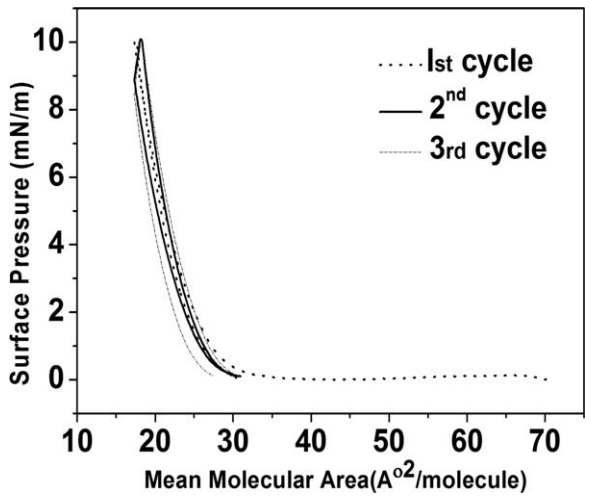

Figure 4. π-*A* multiple isotherms profile of PANi–TiO_2 (20 wt %) nanocomposite monolayer, particle concentration 0.2 mg/mL in NMP solution, spreading amount 200 μL, target pressure 10 mN/m, rate 10 mm^2/min, and no. cycles are 3.

respectively. The 320 nm band is attributed to a π-π^* transition in the benzenoid ring. The absorption in the visible range, at 630 nm, is attributed to the π–polaron transition in the quinoid rings. The spectra are characteristic for the emeraldine base formed upon the deprotonation action of NMP on the PANi salt. Excess of NMP leads to deprotonation of the salt to emeraldine base. This is due to the C═O groups in NMP that forms hydrogen bonds with the dopant acid and inhibits the doping process.[33,34]

The position of the 630 nm absorption band is little shifted in PANi–TiO_2 nanocomposites with variation in concentration of TiO_2. In PANi–TiO_2 (20 wt %) nanocomposites, the peak at 320 nm shifts to 340 nm and 630 nm shits to 648 nm and this broad absorption band follows a long tail in the visible-light region. The tail is indicative of charge carrier delocalization in the polaron band favored by an extended chain conformation of the PANi. Therefore, PANi–TiO_2 nanocomposites can be excited to produce more electron–hole pairs under visible-light illumination and this is expected to increase photocatalytic activities.[35] As there is little red shift in case of PANi–TiO_2 (20 wt %) nanocomposites, so we choose it for further investigations.

The UV–Vis spectra of LB film of 25 layers of PANi–TiO_2 (20 wt %) nanocomposites on quartz substrate is shown in Figure 5(ii). The two electronic transitions at 320 nm and 604 nm are observed. These peaks arise due to the transition from a polaron to bipolaron lattice. UV–Vis results indicated that film transferred from pure water surface is in the emeraldine base state.[36] The position of the 630 nm absorption band is little shifted with film thickness. Similar peaks were observed in single monolayer but with very low intensity. The absorbance peak increases with the number of deposited layers indicating that a suitable multilayer build-up is accomplished.

X-ray Diffraction. Figure 6(i) shows the X-ray diffraction profile of PANi, Pure TiO_2 nanoparticles, and PANi–TiO_2 (5, 10, 15, 20 wt %) nanocomposites when exposed to Cu-k_α radiation source from X-ray diffractometer (Philips XPERT-PRO MPD). Most forms of PANi are amorphous and show the presence of broad high-angle asymmetric scattering peaks stretching from 2θ between 15° and 25°. The peaks of the synthesized PANi show broad peaks (of less intensity) situated at $\sim 2\theta = 21.23°$ and 25.15° corresponding to d-spacing of 4.184 Å and 3.54 Å. It indicates the presence of benzene rings and polymeric nitrogen. This d-space is the characteristic distance between the planes of benzene rings in adjacent planes and is the interchain or the close contact distance between two adjacent chains.

X-ray diffraction peaks for the TiO_2 nanoparticles were observed at $2\Theta = 25.24°$, 37.76°, 48.01°, 53.86°, 54.97°, 62.65°, 68.80°, 70.19°, and 75.08°. They were assigned (101), (004), (200), (105), (211), (201), (116), (220), and (215) diffraction

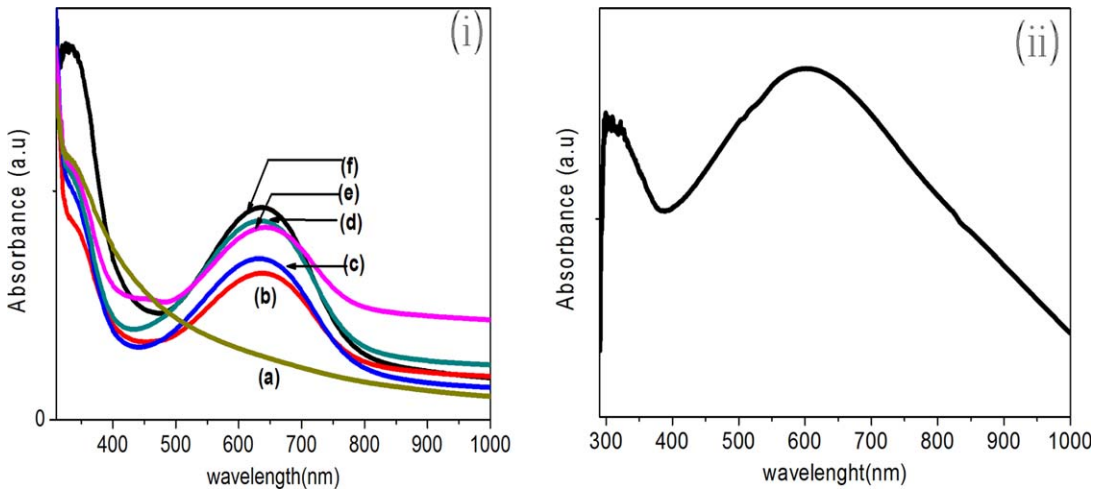

Figure 5. (i) UV–visible spectra of the (a) TiO_2 nanoparticles, (b) 5, (c) 10, (d) 15, (e) 20 wt % TiO_2 in PANi–TiO_2 nanocomposite, respectively, and (f) pure PANi; (ii) UV–visible spectrum of LB film of 25 layers of PANi–TiO_2 (20 wt %) nanocomposite deposited on quartz substrate. [Color figure can be viewed in the online issue, which is available at wileyonlinelibrary.com.]

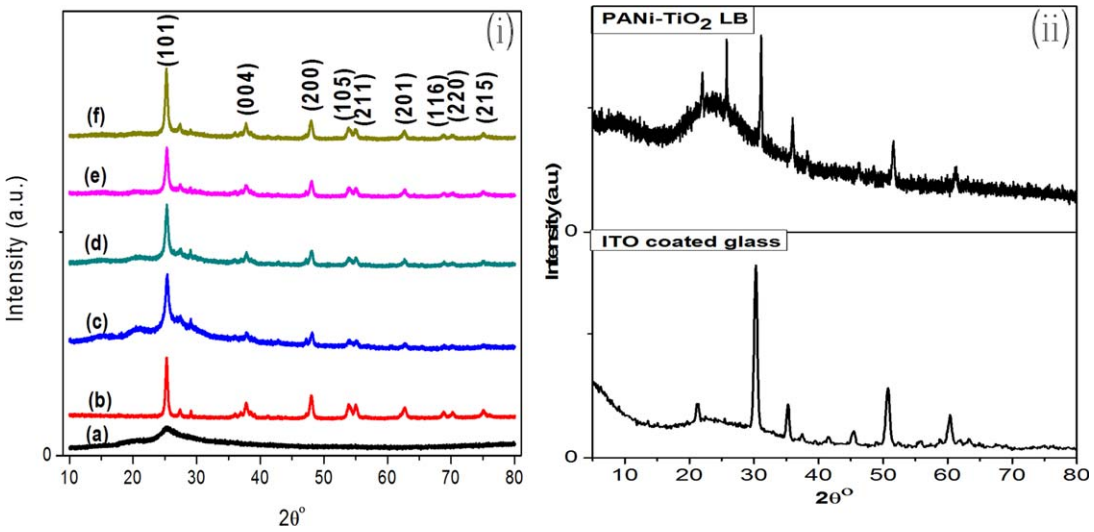

Figure 6. (i) XRD profile of (a) pure PANi, (b) TiO_2 nanoparticles, (c) 5, (d) 10, (e) 15, and (f) 20 wt % TiO_2 in PANi–TiO_2 nanocomposite. (ii) XRD pattern of ITO-coated glass and LB film of 25 layers of PANi–TiO^2 (20 wt %) nanocomposite deposited on ITO glass substrate. [Color figure can be viewed in the online issue, which is available at wileyonlinelibrary.com.]

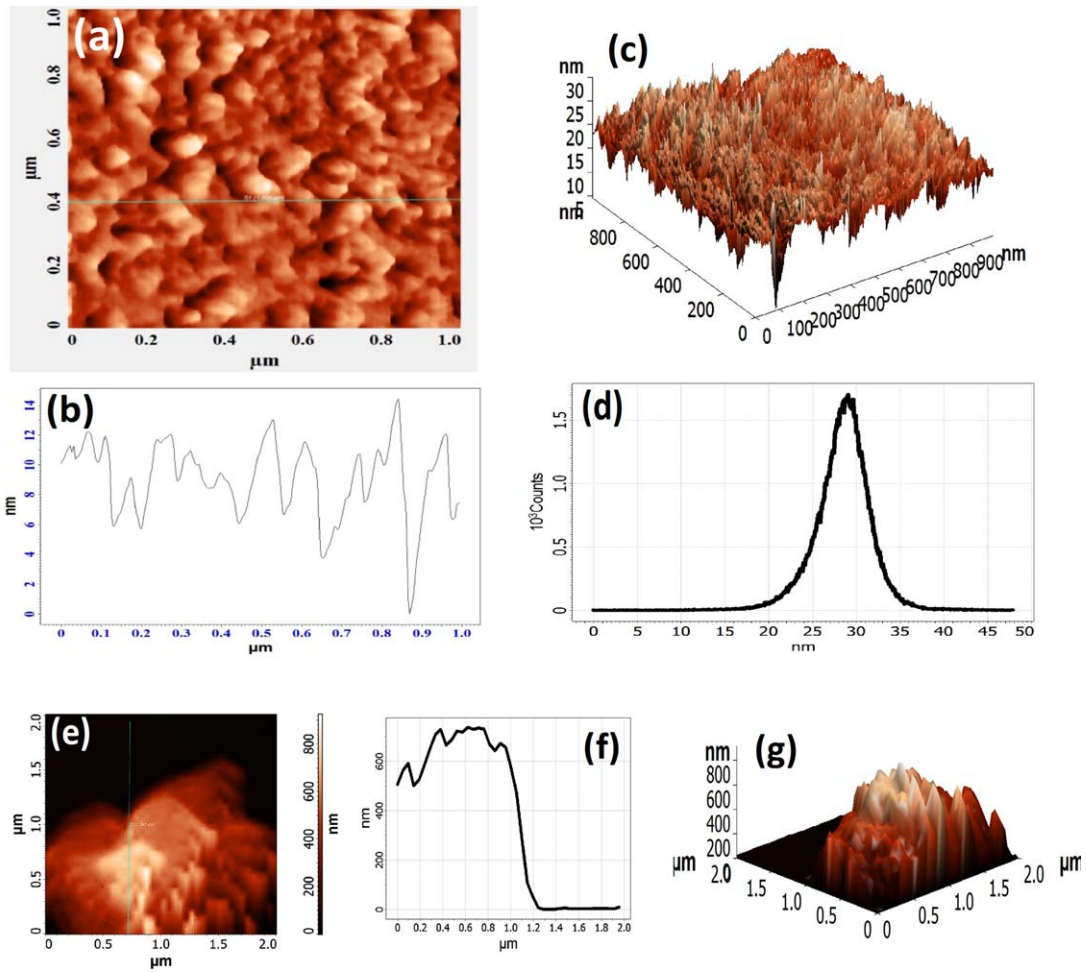

Figure 7. (a) AFM image of PANi–TiO_2 (20 wt %) nanocomposite LB film deposited on the quartz substrate, (b) the corresponding height profile, (c) its 3D image and (d) count of particle size distribution, (e) AFM image of edge of LB film of 25 layers of PANi–TiO_2 (20 wt %) nanocomposite, (f) the corresponding height profile and (g) 3D image. [Color figure can be viewed in the online issue, which is available at wileyonlinelibrary.com.]

peaks of anatase TiO_2. All peaks are in good agreement with the standard spectrum (JCPDS no.: 21–1272). Figure 6(i) shows XRD patterns for 5, 10, 15, 20 wt % TiO_2 in PANi–TiO_2 nanocomposite, respectively, exhibiting strong diffraction peaks at $2\Theta = 25.23°$, 37.73°, 48.07°, 53.86°, 54.83°, 62.59°, 68.79°, 70.15°, and 75.06°. The hybrid component materials show the characteristics of both PANi and TiO_2. With increasing TiO_2 percentage in the composite, the intensity of the broad peak of PANi is decreased. The average particle size of PANi–TiO_2 (20 wt %) nanocomposite is found to be 29 nm using Debye-Scherrer's equation,

$$\tau = K\lambda/\beta\cos\theta$$

where K is the shape factor, λ wavelength of X-ray, β is the line broadening at half the maximum intensity (Full Width at Half Maximum) in radians, and θ is the Bragg's angle.[37]

Figure 6(ii) shows X-ray diffraction patterns of the ITO coated glass substrate revealing peaks at $2\Theta = 21.66°$, 30.52°, 35.52°, 37.68°, 50.78°, and 60.72° (JCPDS Card No. 06–0416). They were assigned (211), (222), (400), (411), (440), and (622) diffraction peaks of ITO film.[38,39] The XRD pattern of the LB film of 25 layers PANi–TiO_2 (20 wt %) nanocomposite deposited ITO-coated glass, illustrated in Figure 6(ii), shows the peaks at $2\Theta = 21.75°$, 25.72°, 30.89°, 35.94°, 48.22°, 50.78°, and 62.59°. The peaks at $2\Theta = 25.72°$, 48.22°, and 62.5° can be indexed to the anatse TiO_2 phase. The intensity of peaks of ITO at $2\Theta = 21.75°$, 30.89°, 35.94°, and 50.78° is dampened.

The thickness of LB film of 25 layers is found to be 700 nm using Debye-Scherrer's equation.

Atomic Force Microscopy of Nanocomposite Films

The PANi–TiO_2 nanocomposite LB film was scanned under atomic force microscope (AFM) (Solver-NEXT NT-MDT; Zelenograd, Moscow, Russia) equipped with Silicon nitride (SiN) probe in noncontact mode. It has tip curvature radius 6 nm, attached to a cantilever having resonance frequency (87–230 kHz), and force constant 5.1 mN/m. The quartz substrate was initially scanned under AFM and root mean square (RMS) roughness <1 nm was observed which ensures the smoothness of the quartz and its suitability for deposition of the monolayer. Figure 7(a) shows AFM image (512 × 512 pixels) of PANi–TiO_2 (20 wt %) nanocomposites monolayer on the quartz substrate. Its corresponding height profile and its three-dimensional (3D) view is shown in Figure 7(b,c), respectively. The scan range was 1 μm × 1 μm and scan rate was 1 Hz. Surface roughness average was 2.02 nm and RMS roughness was 2.67 nm. We noted that the PANi–TiO_2 monolayer surface roughness is smooth at a molecular level and is composed of pebble-like protrusions. The monolayer microscopic structure is formed from nanometer-scale grains. We find maximum number of counts of particles having size ~29 nm as shown in Figure 7(d).[40] Figure 7(e) shows the image of edge of the LB film of 25 layers of PANi–TiO_2, scan range 2 μm × 2 μm. The height profile shows the approximate height is about 700 nm (along Z-axis) up to 1.2 μm then after that height profile reaches nearly zero indicating the surface of quartz as shown in Figure 7(f). Figure 7(g) shows 3D image of edge of the LB film of 25 monolayer of PANi–TiO_2 which also shows the height of LB film of 25 layers from above the quartz surface.[41]

CONCLUSION

We succeeded in preparing and characterizing the ultrathin self-assembled films of PANi–TiO_2 nanocomposites. FTIR study shows the presence of both TiO_2 and PANi molecules in of PANi–TiO_2 nanocomposites, whereas XRD study confirmed the anatase phase and particle size of PANi–TiO_2. Electronic structure of PANi–TiO_2 and its LB film is confirmed by UV–Vis spectroscopy. Surface pressure–area isotherms indicate an increase in condensed area of PANi–TiO_2 over PANi molecules at the air–water interface. The investigation revealed the inclusion of TiO_2 in the polymer matrix, which occurs during the film formation. Morphology of PANi–TiO_2 nanocomposite LB films shows that they are formed from nanometer-size grains. We are further investigating the electrical properties of PANi–TiO_2 nanocomposite LB films. The possibility of manipulation of the material size and shape by LB technique is of great importance for a better use of conducting properties, thus extending its applications. This work is highly useful for sensor device fabrication technology.

ACKNOWLEDGMENTS

The authors (G.K.B. and R.K.) acknowledge the financial support from University Grants Commission, India in terms of a Senior Research Fellowship. They also thank Ms. L.K. Brar for many helpful discussions during the course of this work.

REFERENCES

1. Dai, L. In Engineering Materials and Processes Series; Derby, B., Ed.; Springer: London, **2004**; Vol. 1, p 266.
2. Mike, J. F.; Lutkenhaus, J. L. *J. Polym. Sci. Part B: Polym. Phys.* **2013**, *51*, 468.
3. Lodha, A.; Kilbey, S. M., II.; Ramamurthy, P. C.; Gregory, R. V. *J. Appl. Polym. Sci.* **2001**, *82*, 3602.
4. Silveira, F. Z.; Duarte, G. W.; Tachinski, C. G.; Piletti, R.; Fiori, J, Jr.; Peterson, M.; Riella, H. G.; Fiori, M. A. *J. Appl. Polym. Sci.* **2013**, *128*, 430.
5. Singh, A. K.; Dwivedi, A. D. D.; Chakrabarti, P.; Prakash, R. *J. Appl. Phys.* **2009**, *105*, 114506.
6. Pandey, R. K.; Takashima, W.; Nagamatsu, S.; Dauendorffer, A.; Kaneto, K.; Prakash, R. *J. Appl. Phys.* **2013**, *114*, 054309.
7. Gurunathan, K.; Trivedi, D. C. *Mater. Lett.* **2000**, *45*, 262.
8. Bhandari, H.; Sathiyanaranayan, S.; Choudhary, V.; Dhawan, S. K. *J. Appl. Polym. Sci.* **2009**, *111*, 2328.
9. Dey, A.; De, S.; De, A.; De, S. K. *Nanotechnology* **2004**, *15*, 1277.
10. Xiong, S.; Wang, Q.; Chen, Y. H. *Mater. Chem. Phys.* **2007**, *103*, 450.
11. Ansari, M. O.; Mohammad, F. *J. Appl. Polym. Sci.* **2012**, *124*, 4433.
12. Savitha, K. U.; Gurumallesh, P. H. *J. Appl. Polym. Sci.* **2013**, *127*, 3147.
13. Gurunathan, K.; Amalnerkar, D. P.; Trivedi, D. C. *Mater. Lett.* **2003**, *57*, 1642.

14. Huyen, D. N.; Tung, N. T.; Thien, N. D.; Le, T. H. *Sensors* **2011**, *11*, 1924.
15. Pawar, S. G.; Patil, S. L.; Chougule, M. A.; Raut, B. T.; Pawar, S. A.; Patil, V. B. *Sens. Transducers J.* **2011**, *125*, 107.
16. Zhang, X.; Yan, G.; Ding, H.; Shan, Y. *Mater. Chem. Phys.* **2007**, *102*, 249.
17. Wang, F.; Xiong, S. M. *Chin. Chem. Lett.* **2007**, *18*, 1273.
18. Singh, A. K.; Chakrabarti, P.; Prakash, R. *IEEE Electron Device Lett.* **2011**, *32*, 5.
19. Singh, A. K.; Prakash, R. *RSC Adv.* **2012**, *2*, 5277.
20. Pandey, R. K.; Singh, A. K.; Prakash, R. *AIP Adv.* **2013**, *3*, 122120.
21. Dhanabalan, A.; Riul, A.; Mattoso, L. H. C., Jr.; Oliveira, O. N., Jr. *Langmuir* **1997**, *13*, 4882.
22. Tanami, G.; Gutkin, V.; Mandler, D. *Langmuir* **2010**, *26*, 4239.
23. Prabhakar, N.; Matharu, Z.; Malhotra, B. D. *Biosens. Bioelectron.* **2011**, *26*, 4006.
24. Manigandan, S.; Majumder, S.; Ganguly, S.; Kargupta, K. *Mater. Lett.* **2008**, *62*, 2758.
25. Dhanabalan, A.; Dabke, R. B.; Kumar, N. P.; Talwar, S. S.; Major, S.; Lal, R.; Contractor, A. Q. *Langmuir* **1997**, *13*, 4395.
26. Granholm, P.; Paloheimo, J.; Stubb, H. *Phys. Scr.* **1997**, *69*, 146.
27. Colthrop, N. B.; Daley, L. H.; Wiberley, S. E. Introduction to Infrared and Raman Spectroscopy; Academic Press: San Diego, CA, **1990**; Chapter 11, p 339.
28. Bellamy, L. J. Infrared Spectra of Complex Molecules; Chapman & Hall: New York, **1980**; Vol. 2, p 24.
29. Wu, R. J.; Sun, Y. L.; Lin, C. C.; Chen, H. W.; Chavali, M. *Sens. Actuators A* **2006**, *115*, 198.
30. Wei, J.; Zhang, Q.; Liu, Y.; Xiong, R.; Pan, C.; Shi, J. *J. Nanopart. Res.* **2011**, *13*, 3157.
31. Pandey, R. K.; Upadhyay, C.; Prakash, R. *RSC Adv.* **2013**, *3*, 15712.
32. Kaur, R.; Bhullar, G. K.; Raina, K. K. *Liq. Cryst.* **2012**, *39*, 1375.
33. Chen, S. A.; Lee, H. T. *Macromolecules* **1993**, *26*, 3259.
34. Pruneanu, S.; Veress, E.; Marian, I.; Oniciu, L. *J. Mater. Sci.* **1999**, *34*, 2733.
35. Xia, H.; Wang, Q. *J. Appl. Polym. Sci.* **2003**, *87*, 11.
36. Oliveira, O. N., Jr.; Raposo, M.; Dhanabalan, A. In Solid Thin Films and Layers; Nalwa, H. S., Ed.; Elsevier: Academic Press, **2001**; Vol. 4, Chapter 1, p 21.
37. Prasanna, G. D.; Jayanna, H. S.; Prasad, V. *J. Appl. Polym. Sci.* **2011**, *120*, 2856.
38. Deng, W.; Ohgi, T.; Nejo, H.; Fujita, D. *Appl. Phys. A* **2001**, *72*, 595.
39. Kang, S. B.; Lim, J. W.; Lee, S.; Kim, J. J.; Kim, H. K. *J. Phys. D: Appl. Phys.* **2012**, *45*, 325102.
40. Kaur, R.; Raina, K. K. *Liq. Cryst.* **2014**, *41*, 1065.
41. Zhang, J.; Burt, D. P.; Whitworth, A. L.; Mandler, D.; Unwin, P. R. *Phys. Chem. Chem. Phys.* **2009**, *11*, 3490.